In-situ deformation modulus of rust in concrete under different levels of confinement and rates of corrosion

Qifang Liu[a], Ray Kai Leung Su[b1], Chun-Qing Li[c], Kaimin Shih[b], Changzhong Liao[b]

[a]*Institute of Urban Smart Transportation & Safety Maintenance, Shenzhen University, Shenzhen, PRC*
[b]*Department of Civil Engineering, The University of Hong Kong, Pokfulam Road, Hong Kong, PRC*
[c]*School of Engineering, RMIT University, Melbourne, Vic 3001, Australia*

Abstract: The large uncertainty of the value of the deformation modulus of rust in the literature and the granular property of rust make it difficult to correctly simulate the interaction between the corroded reinforcement and concrete, including rust expansion and bond slip behavior. To fill the gap, this study thereby quantifies the deformation modulus of rust in concrete under different levels of confinement, and takes into consideration the effect of the corrosion rate through an in-situ testing method. To obtain a more accurate deformation modulus of rust, the chemical composition and quantity of rust are examined by using X-ray diffraction. Moreover, the effect of diffusion of rust into concrete porous zone and crack was incorporated into the compressive deformation of rust. The results show new empirical relationships between the deformation modulus of rust and the confinement pressure together with the corrosion rate are obtained. These relationships are further validated by the test results in the literature. The present work can contribute to narrow the uncertainties in the deformation modulus of rust for simulating and predicting the deterioration of concrete structures due to reinforcement corrosion.

Keywords: In-situ deformation modulus; rust; steel reinforced concrete; corrosion; X-ray diffraction

1. Introduction

Corrosion of reinforcement can produce expansive stress in the concrete due to a substantial increase of volume when steel is oxidized. The increased stress always

[1] Corresponding author. Tel.:+852 2859 2648
E-mail address: klsu@hku.hk (RKL Su)

causes the cracking of concrete and the decreasing of confinement on reinforcement, thereby reducing the bonding stress between steel reinforcement and concrete [1]. Apart from the reduction of the area of reinforcement, the expansive stress and the loss of bond at steel-concrete interface are considered as two of the main reasons of deterioration of corroded concrete structures [2, 3]. However, it is a challenging task to realistically simulate the expansion of rust and the bond slip behavior at steel-concrete interface because there is a large uncertainty of the deformability of rust in corroded concrete structures [3, 4].

As a primary parameter, the deformability of rust is essential when considering the interaction between steel and concrete, which is a necessary aspect and cannot be neglected for correct evaluation of the behavior of reinforced concrete structures, especially when external loading is considered [2, 3, 5]. The deformability of rust can affect not only the expansion of rust layer but also the bonding stress between the steel rebar and concrete [3, 6, 7]. Previous studies [8-10] have shown that the deformability of rust can greatly affect the accuracy of predicting the time to cover cracking especially when the input parameter is less than 100 MPa.

However, a wide range of values from tens of MPa to several hundreds of GPa of the Young's modulus of rust are reported in the literature [11-20], and no consensus in experimental results is available [3, 6, 12, 14]. Moreover, it has been proved that rust does not behave elastically because rust is a granular material [7, 12, 21]. Therefore, similar to the determination of rock deformability [22], the term *deformation modulus* rather than modulus of elasticity or Young's modulus will be used in the present work to characterize the deformability of rust. As the deformation modulus of rust highly depends on the subjected confinement of concrete resulting from its granular properties [7, 12, 15], it is therefore not enough to only determine the order of magnitude. For realistic simulation, the deformation modulus of rust under different levels of confinement pressure should be predicted. Nevertheless, no method or equation for the prediction has been found in the literature.

Due to the granular properties of rust, the complexity of addressing this research gap involves modeling the deformation behavior of rust with minimal disturbance to the original structural configurations. As rusting is caused by the dissipative interaction among the grains and forming of unique configurations [23, 24], it is difficult to model the granular behavior with rust samples which are collected by damaging corroded reinforced concrete (RC). Therefore, an in-situ testing method is presented in our previous study [20], in which the deformation modulus of rust was investigated by measuring the displacement with digital image correlation (DIC). However, the variation of the deformation modulus of rust in different levels of confinement remains unknown.

This study will thereby focus on the quantification of the deformation modulus of rust under different levels of confinement pressure by surrounding concrete, and take into consideration the effect of the corrosion rate through an accelerated corrosion test. The experimental investigation follows the same procedures as that described in Liu and Su [20] to measure the displacement on concrete surface, whilst both cylindrical specimens and square specimens are tested in the present work. Additionally, the volume expansion coefficient of rust (ratio between volume of rust and iron) is evaluated in this work by examining the chemical composition of rust through X-ray diffraction (XRD) to obtain a more accurate deformation modulus of rust. Finally, in the inverse analysis of the in-situ deformation modulus of rust in the present work, the displacement-based method proposed by Liu and Su [20] is modified. As rust does not behave elastically, its deformation modulus will be evaluated as the ratio of the confinement pressure and the resulting deformation similar to that used in determination of rock deformability [22]. Moreover, the amount of rust diffusion into concrete will be considered as part of the compressive deformation, and thus can be incorporated into the deformation modulus to eliminate errors when approximating the diffusion of rust.

It is noted that in accelerated corrosion tests, similar chemical compositions as those found in natural corrosion environments have been observed in previous studies [19, 25]. However, the microstructure and deformation modulus of rust may differ with corrosion rate and thus the deformation rate, which prompts to consider the effect of corrosion rate in this work. Even though the long-term effects, such as creep, shrinkage, and hardening of concrete which are found in natural corrosion conditions are neglected in accelerated corrosion testing [8, 9], there is no evidence that these effects would affect the deformation modulus of rust. On the other hand, the amount of diffusion and distribution of rust by applying an electric current in accelerated corrosion testing are observed to be different from those in natural corrosion environments [26]. Therefore, the two key parameters which may affect the amount of diffusion of rust, i.e. the porosity of concrete and corrosion rate, will be considered in this work by investigating different concrete strengths and applied current densities.

2. A modified displacement-based inverse analysis method

This study will investigate the deformation modulus of rust under different levels of confinement by the surrounding concrete, and take the effect of the corrosion rate into consideration. The displacement-based inverse analysis method proposed by the authors [20] will be adopted and modified by regarding the diffusion of rust as part of the compressive deformation of rust due to the confinement of concrete, which can eliminate errors when approximating the diffusion of rust. The effect of the diffusion of rust into the porous zone and crack of concrete is therefore incorporated to the deformation modulus of rust.

As shown in Fig. 1, the corrosion of the steel reinforcements causes displacement from the expansion of rust, d_s, at the interface of the concrete and steel because rust (mainly iron oxides) has a greater volume than iron. The diameter of the rebar and thickness of concrete cover are, respectively, D and C. Due to confinement by the surrounding concrete, pressure p develops on the interface which induces cracking in the concrete and compression of the rust (see Fig.1a). The crack front at r_0 divides the concrete into an intact exterior and cracked interior.

Similar to the approach adopted in the Liu and Su [20], the intact component of the concrete is modelled as an isotropic elastic body, whilst the cracked component is modeled as an orthotropic elastic body [27, 28] because the tangential stiffness is reduced due to the strain softening effect from the cracking, whereas the radial stiffness of the concrete remains unchanged. By applying the isotropic elasticity theory to the intact concrete and using orthotropic elastic constitutive equations for the cracked concrete, the tangential stress at radius of r in the intact concrete and cracked concrete are $\sigma_{\theta,1}(r)$ and $\sigma_{\theta,2}(r)$ respectively [20, 28]:

$$\sigma_{\theta,1}(r)=\frac{E_{ef}}{1-\nu_c^2}\left[(1+\nu_c)c_1+(1\text{-}\nu_c)\frac{c_2}{r^2}\right] \tag{1}$$

$$\sigma_{\theta,2}(r)=\frac{\alpha E_{ef}}{1-\nu_c^2}\left[(1+\nu_c)c_3r^{\sqrt{\alpha}-1}+(1-\nu_c)c_4r^{-\sqrt{\alpha}-1}\right] \tag{2}$$

where E_{ef} and ν_c are the effective Young's modulus and Poisson's ratio of the concrete. α is a residual tangential stiffness factor. c_1-c_4 are unknown parameters which can be obtained by solving the equations in Appendix A.

The compressive pressure p at the interface of the concrete and rust can be obtained from a stress equilibrium as:

$$p=\frac{1}{D/2}\left(\int_{D/2}^{r_0}\sigma_{\theta,2}(r)dr+\int_{r_0}^{D/2+C}\sigma_{\theta,1}(r)dr\right) \tag{3}$$

As rust does not behave elastically, the deformability of rust is evaluated by the deformation modulus E_{rust} defined as the ratio between confinement pressure p and the corresponding strain of rust ε including the elastic and inelastic stages [7, 22], i.e.

$$E_{rust}=p/\varepsilon \tag{4}$$

with the strain in rust

$$\varepsilon=\frac{d_{rust}}{\delta+d_0} \tag{5}$$

where the compressive deformation of rust d_{rust} can be determined by applying the displacement compatibility at the concrete/steel interface after the expansion displacement of rust d_s is measured with DIC. As shown in Fig. 1b, free expansion δ is equal to the sum of the expansion displacement d_s, compressive deformation of rust d_{rust}, and thickness of rust due to diffusion into the concrete δ_p, i.e.,

$$\delta=d_s+d_{rust}+\delta_p \tag{6}$$

Assuming that the volume expansion coefficient is *n*, free expansion displacement δ can be expressed as:

$$\delta = \frac{D}{2}\sqrt{1+(n-1)\frac{M_{loss}}{\rho_{st}\pi D^2/4}} - \frac{D}{2} \tag{7}$$

where ρ_{st} is the density of the steel. The mass loss of the steel based on length M_{loss} in *t* years from corrosion is approximated by applying Faraday's law [20]:

$$M_{loss} = 9.127\pi D i_{corr} t \tag{8}$$

where i_{corr} (A/m^2) is the rate of corrosion in the reinforcement.

The thickness of the rust due to diffusion into concrete δ_p can be approximated as [29]:

$$\delta_p = k_T\left(d_s + d_0\right) \tag{9}$$

where d_0 is the radial loss of the steel, i.e.,

$$d_0 = \frac{D}{2}\left(1-\sqrt{1-\frac{M_{loss}}{\rho_{st}\pi D^2/4}}\right) \tag{10}$$

By accelerating the corrosion of specimens through wetting and drying cycles coupled with galvanic current, the value of k_T was observed to range from 0.3 to 0.525, depending on the strength of the concrete and its porosity [29]. In the present study, as the corrosion of reinforcement was solely accelerated with electric current, the value of k_T may have a large difference.

In the previous displacement-based inverse analysis method proposed by the authors [20], the compressive deformation of rust d_{rust} can be evaluated by

$$d_{rust} = \delta - d_s - \delta_p \tag{11}$$

where δ is calculated by Eq. (7), d_s can be measured with DIC.

However, errors may come from the approximation of δ_p as given in Eq. (9) because the value of k_T is unknown. The value of k_T can greatly affect the accuracy of E_{rust} as discussed in section 5. Therefore, to eliminate errors when approximating k_T and δ_p, the amount of the diffused rust into concrete is considered to be a mechanical behavior of rust as part of the compressive deformation of rust in the present study, i.e.

$$\bar{d}_{rust} = d_{rust} + \delta_p = \delta - d_s \tag{12}$$

where $\bar{d}_{rust}$ is the compressive deformation of rust that takes the diffused rust into consideration. The deformation modulus of rust $\bar{E}_{rust}$ is obtained by substituting $\bar{d}_{rust}$ into Eq. (4) and (5).

Lundgren [7] noted that the diffusion of rust can be regarded as a mechanical behavior as well. The main arguments are: (i) there is little rust that diffuses into concrete when the corrosion of the reinforcement is accelerated by using a high current density [7]. E_{rust} and $\bar{E}_{rust}$ should have close values in this case; (ii) the diffused rust only reduces d_s and has no effect on the mechanical behavior of rust. By including the diffusion of rust as a mechanical property of rust, the errors for calculating δ_p and the subsequent d_{rust} can be eliminated; and (iii) both the diffusion of rust and the mechanical behavior of rust depend on the corrosion rate and properties of concrete [7, 16, 30], such as the compressive and tensile strengths of concrete, porosity, etc. By investigating the changes in $\bar{E}_{rust}$ with the corrosion rate and concrete strength, the diffusion of rust can be incorporated back as part of the d_{rust} for simulating the natural corrosion of reinforcements.

Section 5 will further investigate the effect of k_T and δ_p on the results of E_{rust} to show the necessity to incorporate the diffusion of rust into the compressive deformation of rust. The rationality will be validated by employing the findings of $\bar{E}_{rust}$ for prediction of the accelerated corrosion test and the natural corrosion test in the literature.

3. Experimental scheme

3.1. Specimen

To examine the variations in the deformation modulus of rust versus confinement of concrete and corrosion rate, experiments were carried out to measure the displacement on the concrete surface induced by the expansion of rust. Cylindrical specimens with dimensions of 100 mm × 50 mm or square columns of 100 mm × 100 mm × 50 mm (see Fig. 2) were prepared for accelerated corrosion testing. An as received hot-rolled rebar was embedded into the center of the concrete. The rebar diameter is 12 or 16 mm. The different levels of confinement of concrete are simulated by casting the concrete with different water to cement ratios (w/c; 0.4, 0.46, 0.54, and 0.7). The concrete specimens were mixed and cast in the laboratory at the University of Hong Kong. The Portland cement CEM I 52.5N was used for concrete casting. The maximum size of the aggregate was 10 mm. To obtain the material properties, three standard concrete cubes and two standard cylinders were cast for determining the cube compressive strength f_{cu}, the static modulus of elasticity in compression E_c and the splitting tensile strength f_t in accordance with Hong Kong construction standard CS1 [31]. After being cast and cured for 28 days, the specimens were placed in air until corrosion test (temperature: 20 ± 2 °C; relative humidity: 75–85%). The tested mechanical properties of the concrete after 28-days of curing are provided in Table 1.

3.2. Accelerated corrosion test

As shown in Fig. 3, corrosion of the reinforcement is accelerated by applying the galvanostatic method. A constant current density was applied with a current regulator onto the steel rebar. For a reliable connection, a wire that was routed from the current regulator was tightened onto the top of the rebar with a screw. During the corrosion process, the rebar acted as the anode, and a graphite rod (counter electrode) was placed in a sodium chloride (NaCl) solution as the cathode [32, 33]. The commonly used nominal current density is 200 μA/cm^2. To investigate the variations in the deformation modulus of rust with corrosion rate, the impressed current densities on Specimens U1-11 were changed from 100 μA/cm^2 to 676.5 μA/cm^2. The test parameters of the specimens are listed in Table 1.

Prior to the corrosion test, the specimen was immersed into a 3.5% NaCl solution by weight of water with about 2 mm of the specimen above the surface of the solution. This was done because chloride ions can quickly transport with water through concrete cover to arrive at the surface of reinforcement, and thus the active corrosion state of reinforcement can be initiated. To prevent rust escaping from the bottom surface which can lead to release of expansive pressure, the bottom of the specimen was sealed with epoxy resin (see Fig. 2).

The accelerated corrosion of the reinforcement was recorded along with the displacement from the expansion of rust d_s by using DIC. The camera and specimen were fastened onto an optical plate through a support frame to reduce the impacts of potential vibrations and disturbance from the surrounding environment. To reduce flickering from the illumination lighting, two LED lights powered with a constant current were installed. These are mainly done to increase the accuracy of the measurements when using DIC. Speckle patterns were generated on the surface of the specimens to capture and simulate the deformation of the digitally recorded images. To investigate the volume expansion coefficient, rust was collected after testing to examine the components by carrying out an XRD analysis.

Three specimens were tested under current densities higher than 200 μA/cm^2. The test generally took 3 to 10 days until visible crack of concrete cover, which was dependent on the applied current densities and concrete properties. For the current densities of 100 μA/cm^2 and 200 μA/cm^2, only two specimens were tested because the duration varied from 15 days to 33 days. The results were averaged for presentation and discussion. During corrosion test, the level of NaCl solution was kept the same by regularly adding water into the solution.

4. Volume expansion coefficient

The volume expansion coefficient of rust n is a critical parameter when evaluating the deformation modulus of rust, which can be determined by analyzing the constituents of rust. The rust produced in U1 was collected by breaking up the specimen after conducting the accelerated corrosion test, and subsequently examined through an XRD analysis.

According to Francois et al. [34], the primary iron oxides in reinforcements that might form in concrete, i.e. goethite (α-FeO(OH)), magnetite (Fe_3O_4), lepidocrocite (γ-FeO(OH)) and akaganeite (β-FeO(OH)), depend on the chloride content. The measured XRD spectra of the collected rust are shown in Fig. 4. It can be observed that the rust is mainly composed of goethite and magnetite, as well as some lepidocrocite. It can also be observed that even though the main peaks of hematite (Fe_2O_3) partly overlap with those of goethite and magnetite, the characteristic peaks of hematite at 24.2° and 49.5° are not found in the measured XRD pattern [35]. This is also observed in the XRD patterns in previous studies [16, 19, 25, 36]. Thus, the observed components of rust are mainly goethite, magnetite and lepidocrocite, which is similar to the observed rust components in reinforced concrete [16, 19, 25, 34, 36]. The quantitative XRD (QXRD) analysis results based on Rietveld refinement method [37-39] are shown in Table 2. The mass fraction of goethite, magnetite and lepidocrocite are, respectively, 66.94%, 26.33%, and 6.73%. The volume expansion coefficient of the i^{th} component n_i can be determined by using:

$$n_i = \frac{V_i}{V_{Fe}} \tag{13}$$

where V_i and V_{Fe} are the volume of the i^{th} component of rust and iron, respectively. Assuming that one mole of iron can produce k_i mole of the i^{th} constituent of rust, then Eq. (13) can be rewritten as:

$$n_i = \frac{V_i}{V_{Fe}} = \frac{k_i M_i / \rho_i}{M_{Fe} / \rho_{Fe}} \tag{14}$$

where M_i and M_{Fe} are the molecular weight of the i^{th} constituent of rust and iron, respectively. ρ_i and ρ_{Fe} are the density of the i^{th} constituent of rust and iron, respectively. The M_i, M_{Fe}, ρ_i and ρ_{Fe} of goethite, magnetite, and lepidocrocite can be found in a handbook on iron oxides by Cornell and Schwertmann [40]. The n_i of goethite, magnetite, and lepidocrocite is provided in Table 2 [19].

As a result, the volume expansion coefficient n is [25, 36],

$$n = \sum_{i=1}^{g} \eta_i n_i \tag{15}$$

where g is the total number of constituents of rust. η_i is the mass fraction of the i^{th}

constituent. The volume expansion coefficient n is determined to be 2.7 based on Eq. (15), which is close to that in Zhang et al. [25] (2.43) and Zhao et al. [36] (2.64-3.24). It should be noted that the rust in Zhang et al. [25] was produced by accelerating corrosion with a current, while that in Zhao et al. [36] was collected from natural corrosion conditions in different environments.

5. In-situ deformation modulus of rust

5.1. Results

As mentioned in Section 2, the in-situ deformation modulus of rust can be determined by using the calculated expansion of rust d_s which can be evaluated from the displacement field obtained by using DIC. Fig. 5 shows the measured displacement of U5 in the X- and Y-directions at the time of cover cracking. The discontinuity of the displacement field indicates the initiation of cracking. Multiple pairs of symmetrical points around the circumference of the steel were used to calculate the expansion of rust which is determined by calculating the average of the relative displacement between each pair of symmetrical points d_i.

The non-uniformity of reinforcement corrosion [41] can be evaluated by the ratio of the maximum and average displacement surrounding the perimeter of reinforcement. Though the reinforcement corrosion of square specimens is expected to be less uniform and thus may affect the determination of deformation modulus of rust, it is found that the non-uniformity of square specimens varies from 1.07 to 1.49, whist the values vary from 1.1 to 1.58 for the cylindrical specimens. Compared to the applied current densities and concrete properties, the specimen geometry seems to have insignificant effects on the uniformity of corrosion and the determination of deformation modulus of rust through accelerated corrosion test.

Fig. 6 shows the variations of p and E_{rust} with time in U1. The volume expansion coefficient is determined to be n = 2.7 in Section 4. k_T is considered as 0.4. It can be observed that E_{rust} first increases and then decreases after reaching the peak value. The time at the peak of E_{rust} and p is very close to the time that cover of concrete cracks. The change in E_{rust} with time is obviously in agreement with that of p, which shows that the deformation modulus of rust is highly dependent on the compressive pressure.

To investigate the effect of the approximation of k_T and δ_p on the value of E_{rust}, parametrical study is conducted. Fig. 7 shows the change of evaluated E_{rust} with p in U1 for different parameters of k_T, in which E_{rust} increases with p in the loading stage until the maximum compressive pressure is reached. At the unloading stage, E_{rust} decreases with reduced compressive pressure p. This is typical behavior of the mechanical properties of granular materials, i.e., the stiffness increases with the stress level [7, 12, 21, 23, 42, 43]. It is observed from Fig. 7 that rust does not behave elastically because the release of stress from rust does not restore its initial dimension. This supports to regard rust as a granular material and the usage of the term *deformation modulus* to characterize the relationship between the confinement pressure and the resulting deformation similar to that used in determination of rock deformability [22].

As shown in Fig. 7, the evaluated deformation modulus of rust in U1 by considering different k_T is compared. It is found that the value of E_{rust} increases largely with the increasing of k_T. This is because the approximated δ_p increases while the calculated d_{rust} decreases when taking a larger value of k_T. As a consequence, the evaluated value of E_{rust} increases for a fixed pressure p. The approximation of k_T and δ_p can greatly affect the accuracy of E_{rust}. Thereby, to eliminate the errors when calculating δ_p and d_{rust}, the diffusion of rust δ_p will be incorporated into d_{rust} when quantifying E_{rust} and incorporated back when simulating the natural reinforcement corrosion. In the present work, the deformation modulus of rust $\bar{E}_{rust}$ under different levels of confinement and rate of corrosion will be investigated.

As mentioned in Fig. 6, the $\bar{E}_{rust}$ and p varies with the time and depends on the degree of corrosion. The moment when cover of concrete finally cracks is the most significant when simulating the corrosion induced deterioration of concrete. The $\bar{E}_{rust}$ of U1-U11 at the time of cover cracking (defined as $\bar{E}_{rust}^{cr}$) is thereby evaluated as shown in Table 3. It can be observed that the maximum $\bar{E}_{rust}^{cr}$ of all of the specimens is 50.02 MPa, which is very similar to the observed value in Xu et al. [16] and Konopka [18]. In addition, similar E_{rust} values were also observed by Caré et al. [19] (less than 130 MPa) and Zhao et al. [15] (160 MPa).

Fig. 8(a) shows the changes in $\bar{E}_{rust}^{cr}$ with i_{corr}. It can be observed that $\bar{E}_{rust}^{cr}$ tends to linearly increase with i_{corr}. The trend of $\bar{E}_{rust}^{cr}$ which varies with the strength of the concrete is shown in Fig. 8(b). The compressive strength of the concrete f_{cu} is used to represent the strength of concrete. As shown in Fig. 8(b), the value of $\bar{E}_{rust}^{cr}$ increases with the increasing of f_{cu}. Considering that $\bar{E}_{rust}^{cr}$ depends on the confinement pressure, a linear relationship between p_{cr}, i_{corr} and $\bar{E}_{rust}^{cr}$ is proposed as in Eq. (16):

$$\bar{E}_{rust}^{cr} = 6.3226 + 0.02323 i_{corr} + 1.1618 p_{cr} \tag{16}$$

where p_{cr} is the compressive pressure on the rust at the time of cover cracking. The goodness of fit value of Eq. (16) is 0.85.

5.2. Validation

By applying Eq. (16), the predicted $\bar{E}_{rust}^{cr}$ and that of the experiments are compared in Table 3. It is shown that the predicted and experimental $\bar{E}_{rust}^{cr}$ are in good agreement for most of the specimens. To validate the accuracy of Eq. (16), the critical corrosion depth of the reinforcement $d_{0,crit}$ is predicted by substituting $\bar{E}_{rust}^{cr}$ in Eq. (16) into Eqs. (4)-(10). As the diffusion of rust has been incorporated into $\bar{E}_{rust}^{cr}$ in Eq. (16), δ_p can be incorporated into d_{rust} by using Eq. (12). This can eliminate the errors in $d_{0,crit}$ from estimating the δ_p.

To validate the accuracy of $\bar{E}_{rust}^{cr}$ when estimated by using Eq. (16), the predicted $d_{0,crit}$ and experimental $d_{0,crit}$ in previous studies [44-48] are compared as shown in Fig. 9. It is found that all the values are close to the ideal prediction line, i.e. the line when the predicted $d_{0,crit}$ equals the experimental $d_{0,crit}$, which indicates a good performance in predicting $d_{0,crit}$. The details of the parameters of specimens in previous studies are presented in Table 4. Some of the missing mechanical properties of concrete in Table 4 are calculated with empirical equations [49], i.e. $f_t = 0.53\sqrt{f_{cu}}$ and $E_c = 4600\sqrt{f_{cu}}$. The $d_{0,crit}$ from the prediction and experiments are shown in Table 5. Although the maximum absolute relative error is 16.2%, the average absolute relative error of the predicted $d_{0,crit}$ is 10.1%.

As shown in Table 5 and Fig. 9, a good agreement is also found with the field test results in Torres-Acosta and Sagues [48], in which the corrosion rate varies from 2.7 μA/cm^2 to 6.18 μA/cm^2. This indicates that the value of $\bar{E}_{rust}^{cr}$ in this work can also be applied to simulate and predict the cracking of concrete under natural corrosion conditions.

6. Conclusion

This study has investigated the in-situ deformation modulus of rust in corroded concrete structures under different levels of confinement and rate of corrosion by accelerated corrosion test. The displacement-based inverse analysis method is adopted and modified to eliminate the errors that result from estimating the diffusion of rust. Empirical equations of the deformation modulus of rust under different levels of confinement and corrosion rate are proposed and validated by previous test in the literature. The validation results of the critical depth of reinforcement corrosion by using the predicted deformation modulus of rust correlate well with both of the accelerating corrosion test and the natural corrosion test.

Based on the experimental and analytical studies here, the main conclusions are as follows:

(1) Rust is a granular material which does not deform elastically. The

deformation modulus of rust increases with the compressive pressure;

(2) The deformation modulus of rust at the time of concrete cover cracking increases with corrosion rate and strength of concrete, which can be fitted by the corrosion rate and compressive pressure with a linear relationship;

(3) Rust is mainly composed of goethite, magnetite, and lepidocrocite. The evaluated volume expansion coefficient is 2.7. As the characteristic peaks of hematite (Fe_2O_3) at 24.2° and 49.5° are not found in the measured XRD pattern, hematite is not identified as one of the constituents of rust.

Appendix A

The coefficients c_1, c_2, c_3 and c_4 together with α and the crack front r_0 can be calculated with the following equations:

$$c_1 = \frac{s}{b^2} c_2 \tag{A.1}$$

$$c_2 = \left(1+s\right) \frac{\xi\eta}{\eta-\xi} r_0^{-2\sqrt{\alpha}} c_4 \tag{A.2}$$

$$c_3 = \frac{\xi + s\eta}{\eta-\xi} r_0^{-2\sqrt{\alpha}} c_4 \tag{A.3}$$

$$c_4 = \frac{\left(\eta-\xi\right) a^{\sqrt{\alpha}} d_s}{\left(\eta-\xi\right)+\left(\xi+s\eta\right) a^{2\sqrt{\alpha}} r_0^{-2\sqrt{\alpha}}} \tag{A.4}$$

where

$$\xi = \frac{b^2 r_0^2}{s r_0^2 + b^2} \tag{A.5}$$

$$\eta = \frac{\sqrt{\alpha} b^2 r_0^2}{s\left(r_0^2 - b^2\right)} \tag{A.6}$$

$$s = \frac{1-\nu_c}{1+\nu_c} \tag{A.7}$$

with α and r_0 in the solution of the following equations:

$$c_3 a^{\sqrt{\alpha}} + c_4 a^{-\sqrt{\alpha}} = d_s \tag{A.8}$$

$$\alpha = \frac{1}{\bar{\varepsilon}_\theta} \frac{f_t}{E_{ef}} \exp\left[-\frac{f_t h_c}{G_F}\left(\bar{\varepsilon} - \bar{\varepsilon}_\theta\right)\right] \tag{A.9}$$

where

$$\bar{\varepsilon} = \frac{1}{r_0 - a} \int_a^{r_0} \left(c_1 + c_2 / r^2\right) dr \tag{A.10}$$

$$\bar{\varepsilon}_\theta = \frac{1}{r_0 - a} \int_a^{r_0} \left(c_3 r^{\sqrt{\alpha}-1} + c_4 r^{-\sqrt{\alpha}-1}\right) dr \tag{A.11}$$

References

[1] W.P. Zhang, H. Chen, X.L. Gu, Bond behaviour between corroded steel bars and concrete under different strain rates, Magazine of Concrete Research 68(7) (2015) 364-378.

[2] S. Coccia, S. Imperatore, Z. Rinaldi, Influence of corrosion on the bond strength of steel rebars in concrete, Materials and structures 49(1-2) (2016) 537-551.

[3] B. Šavija, M. Luković, J. Pacheco, E. Schlangen, Cracking of the concrete cover due to reinforcement corrosion: a two-dimensional lattice model study, Construction and Building Materials 44 (2013) 626-638.

[4] B. Sanz, J. Planas, J. Sancho, A closer look to the mechanical behavior of the oxide layer in concrete reinforcement corrosion, International Journal of Solids and Structures 62 (2015) 256-268.

[5] Z. Cui, A. Alipour, Concrete cover cracking and service life prediction of reinforced concrete structures in corrosive environments, Construction and Building Materials 159 (2018) 652-671.

[6] B. Sanz, J. Planas, J.M. Sancho, An experimental and numerical study of the pattern of cracking of concrete due to steel reinforcement corrosion, Engineering Fracture Mechanics 114 (2013) 26-41.

[7] K. Lundgren, Modelling the effect of corrosion on bond in reinforced concrete, Magazine of Concrete Research 54(3) (2002) 165-173.

[8] C. Lu, W. Jin, R. Liu, Reinforcement corrosion-induced cover cracking and its time prediction for reinforced concrete structures, Corrosion Science 53(4) (2011) 1337-1347.

[9] R.K.L. Su, Y. Zhang, A double-cylinder model incorporating confinement effects for the analysis of corrosion-caused cover cracking in reinforced concrete structures, Corrosion Science 99 (2015) 205-218.

[10] K.K. Tran, H. Nakamura, K. Kawamura, M. Kunieda, Analysis of crack propagation due to rebar corrosion using RBSM, Cement and Concrete Composites 33(9) (2011) 906-917.

[11] G. Samsonov, The Oxide Handbook, IFI/Plenum, New York 1973.

[12] A. Ouglova, Y. Berthaud, M. François, F. Foct, Mechanical properties of an iron oxide formed by corrosion in reinforced concrete structures, Corrosion Science 48(12) (2006) 3988-4000.
[13] Y. Zhao, H. Dai, W. Jin, A study of the elastic moduli of corrosion products using nano-indentation techniques, Corrosion Science 65 (2012) 163-168.
[14] B. Šavija, M. Luković, S.A.S. Hosseini, J. Pacheco, E. Schlangen, Corrosion induced cover cracking studied by X-ray computed tomography, nanoindentation, and energy dispersive X-ray spectrometry (EDS), Materials and Structures 48(7) (2015) 2043-2062.
[15] Y. Zhao, H. Dai, H. Ren, W. Jin, Experimental study of the modulus of steel corrosion in a concrete port, Corrosion Science 56 (2012) 17-25.
[16] G. Xu, L. Liu, H. Bao, Q. Wang, J. Zhao, Mechanical properties of steel corrosion products in reinforced concrete, Materials and Structures 50(2) (2017) 115.
[17] K. Suda, S. Misra, K. Motohashi, Corrosion products of reinforcing bars embedded in concrete, Corrosion Science 35(5-8) (1993) 1543-1549.
[18] P. Konopka, Structural properties of rust. 4th-year undergraduate project. Cambridge: University of Cambridge 2005.
[19] S. Caré, Q.T. Nguyen, V. L'Hostis, Y. Berthaud, Mechanical properties of the rust layer induced by impressed current method in reinforced mortar, Cement and Concrete Research 38(8-9) (2008) 1079-1091.
[20] Q.F. Liu, R.K.L. Su, A displacement-based inverse analysis method to estimate in-situ Young's modulus of steel rust in reinforced concrete, Engineering Fracture Mechanics 192 (2018) 114-128.
[21] I. Petre-Lazar, B. Gerard, Mechanical behaviour of corrosion products formed at the steel–concrete interface, Testing and Modelling, EM2000 Proceedings of the 14th Engineering Mechanics Conference, ASCE, Austin, Texas, 2000.
[22] Z.T. Bieniawski, Determining rock mass deformability: experience from case histories, International Journal of Rock Mechanics and Mining Sciences & Geomechanics Abstracts 15(5) (1978) 237-247.

[23] H.M. Jaeger, S.R. Nagel, R.P. Behringer, Granular solids, liquids, and gases, Reviews of modern physics 68(4) (1996) 1259.
[24] F. Radjai, J.-N. Roux, A. Daouadji, Modeling granular materials: century-long research across scales, Journal of Engineering Mechanics 143(4) (2017) 04017002.
[25] X. Zhang, M. Li, L. Tang, S.A. Memon, G. Ma, F. Xing, H. Sun, Corrosion induced stress field and cracking time of reinforced concrete with initial defects: Analytical modeling and experimental investigation, Corrosion Science 120 (2017) 158-170.
[26] H. Wong, Y. Zhao, A. Karimi, N. Buenfeld, W. Jin, On the penetration of corrosion products from reinforcing steel into concrete due to chloride-induced corrosion, Corrosion Science 52(7) (2010) 2469-2480.
[27] S.J. Pantazopoulou, K. Papoulia, Modeling cover-cracking due to reinforcement corrosion in RC structures, Journal of Engineering mechanics 127(4) (2001) 342-351.
[28] C.Q. Li, R.E. Melchers, J.J. Zheng, Analytical model for corrosion-induced crack width in reinforced concrete structures, ACI Structural Journal 103(4) (2006) 479-487.
[29] Y. Zhao, H. Ding, W. Jin, Development of the corrosion-filled paste and corrosion layer at the steel/concrete interface, Corrosion Science 87 (2014) 199-210.
[30] A. Michel, B.J. Pease, A. Peterová, M.R. Geiker, H. Stang, A.E.A. Thybo, Penetration of corrosion products and corrosion-induced cracking in reinforced cementitious materials: Experimental investigations and numerical simulations, Cement and Concrete Composites 47 (2014) 75-86.
[31] Civil Engineering and Development Department of Hong Kong, Construction Standard CS1: Testing Concrete vol. 1, Hong Kong; 1990.
[32] L. Abosrra, A. Ashour, M. Youseffi, Corrosion of steel reinforcement in concrete of different compressive strengths, Construction and Building Materials 25(10) (2011) 3915-3925.

[33] F. Tang, Z. Lin, G. Chen, W. Yi, Three-dimensional corrosion pit measurement and statistical mechanical degradation analysis of deformed steel bars subjected to accelerated corrosion, Construction and Building Materials 70 (2014) 104-117.

[34] R. François, S. Laurens, F. Deby, Corrosion and Its Consequences for Reinforced Concrete Structures, Elsevier 2018.

[35] S. Kabekkodu, PDF-2 2011 (Database), International Centre for Diffraction Data, Newtown Square, PA, USA, 2011.

[36] Y. Zhao, H. Ren, H. Dai, W. Jin, Composition and expansion coefficient of rust based on X-ray diffraction and thermal analysis, Corrosion Science 53(5) (2011) 1646-1658.

[37] H. Rietveld, A profile refinement method for nuclear and magnetic structures, Journal of applied Crystallography 2(2) (1969) 65-71.

[38] C.-Z. Liao, L. Zeng, K. Shih, Quantitative X-ray diffraction (QXRD) analysis for revealing thermal transformations of red mud, Chemosphere 131 (2015) 171-177.

[39] C.-Z. Liao, M. Su, S. Ma, K. Shih, Y. Feng, C. Liu, Y. Ho, Immobilization of lead in cathode ray tube funnel glass with beneficial use of red mud for potential application in ceramic industry, ACS Sustainable Chemistry & Engineering 6(11) (2018) 14213-14220.

[40] R.M. Cornell, U. Schwertmann, The iron oxides: structure, properties, reactions, occurrences and uses, John Wiley & Sons 2003.

[41] Q.F. Liu, R.K.L. Su, A Wasserstein distance-based analogous method to predict distribution of non-uniform corrosion on reinforcements in concrete, Construction and Building Materials 226 (2019) 965-975.

[42] L.D.G. Sigalotti, J. Klapp, E. Sira, Computational and experimental fluid mechanics with applications to physics, engineering and the environment, Springer Science & Business Media 2014.

[43] Y. Gan, M. Kamlah, Discrete element modelling of pebble beds: with application to uniaxial compression tests of ceramic breeder pebble beds, Journal of the

Mechanics and Physics of Solids 58(2) (2010) 129-144.

[44] T. Vidal, A. Castel, R. Francois, Analyzing crack width to predict corrosion in reinforced concrete, Cement and concrete research 34(1) (2004) 165-174.

[45] C. Alonso, C. Andrade, J. Rodriguez, J.M. Diez, Factors controlling cracking of concrete affected by reinforcement corrosion, Materials and structures 31(7) (1998) 435-441.

[46] A.A. Torres-Acosta, Cracking induced by localized corrosion of reinforment in chloride contaminated concrete, University of South Florida, 1999.

[47] C. Andrade, C. Alonso, F.J. Molina, Cover cracking as a function of bar corrosion: Part I-Experimental test, Materials and Structures 26(8) (1993) 453-464.

[48] A.A. Torres-Acosta, A.A. Sagues, Time prediction for concrete cover cracking due to corrosion of embedded reinforcing steel. In: Proc. 6th Ibero-American Corrosion and Protection Congress, 3rd NACE Latin American Region Corrosion Congress and Rehabilitation of Corrosion Damaged Infrastructure, Chapter IV: Modeling Methods, Techniques and Technologies, NACE International; 1998. p. 215–229.

[49] K.A.T. Vu, M.G. Stewart, Structural reliability of concrete bridges including improved chloride-induced corrosion models, Structural safety 22(4) (2000) 313-333.

Table 1 Tested parameters of specimens.

Specimen	f_{cu}	E_c	f_t	i_{corr}	D	C
	MPa	GPa	MPa	μA/cm^2	mm	mm
U1	35.2	22.36	3.29	100	16	42
U2	35.2	22.36	3.29	200	16	42
U3*	30.2	21.8	2.72	500	16	42
U4	43.3	30.49	4.05	200	16	42
U5	52.1	32.07	4.70	200	16	42
U6	35.2	22.36	3.29	300	12	44
U7*	32.1	22.27	3.28	250	16	42
U8*	32.1	22.27	3.28	676.5	16	42
U9*	67	34.1	4.38	500	16	42
U10*	67	34.1	4.38	500	12	44
U11*	30.2	21.75	2.72	500	12	44

*The specimens are square columns.

Table 2 Constituents and mass fraction of rust.

Iron oxide	Volume expansion coefficient [19]	Mass fraction (wt. %)
Goethite α-FeO(OH)	2.91	66.94
Magnetite Fe_3O_4	2.08	26.33
Lepidocrocite γ-FeO(OH)	3.03	6.73

Table 3 Comparison between experimental $\bar{E}_{rust}^{cr}$ and predicted $\bar{E}_{rust}^{cr}$.

Specimen	p_{cr} (exp)	i_{corr}	$\bar{E}_{rust}^{cr}$ (exp)	p_{cr} (pred)	$\bar{E}_{rust}^{cr}$ (pred)	Error
	MPa	μA/cm^2	MPa	MPa	MPa	%
U1	13.65	100	24.03	13.51	24.34	1.30
U2	13.95	200	26.07	13.51	26.67	2.29
U3	13.63	500	36.47	11.4	33.63	-7.77
U4	16.86	200	30.95	16.63	30.29	-2.14
U5	20.02	200	50.02	19.28	33.37	-33.28
U6	16.65	300	29.02	17.51	33.63	15.88
U7	13.15	250	29.51	13.05	27.29	-7.52
U8	13.21	676.5	39.8	13.05	37.19	-6.55
U9	18.33	500	37.9	17.28	38.01	0.30
U10	20.67	500	42.59	22.5	40.08	-5.89
U11	13.33	500	37.48	13.33	33.42	-10.83

Table 4 Parameters of the specimens of previous studies.

Reference	Specimen	D	C	f_{cu}	f_t	E_c	i_{corr}
		mm	mm	MPa	MPa	GPa	μA/cm^2
Vidal et al. [44]	Beam B	12	16	45	4.7	32	10[b]
Alonso et al. [45]	Series-1	16	20	34.8[a]	3.13	27.2[a]	100
	Series-1	16	30	34.8[a]	3.13	27.2[a]	100
Torres-Acosta [46]	CPG1	21	40.5	53	3.86[a]	33.49[a]	100
Andrade et al. [47]	A1	16	30	30	2.9[a]	25.2[a]	100
Torres-Acosta and Sagues [48]	C3	10	34	35	3.14[a]	27.2[a]	5.7
	C4	10	34	37	3.22[a]	27.98[a]	2.7
	C7	10	34	37	3.22[a]	27.98[a]	6.18

[a] The mechanical properties are calculated with empirical equations [49]: $f_t = 0.53\sqrt{f_{cu}}$, and $E_c = 4600\sqrt{f_{cu}}$.

[b] The corrosion rate accelerated by spraying salt fog was assumed to be 10 μA/cm^2.

Table 5 Verification of Eq. (16) by comparing experimental $d_{0,\text{ crit}}$ and predicted $d_{0,\text{ crit}}$.

Reference	Specimen	$d_{s,cr}$ (pred) μm	p_{cr} (pred) MPa	$\bar{E}_{rust}^{cr}$ (pred) MPa	$d_{0,crit}$ (exp) μm	$d_{0,crit}$ (pred) μm	Error %
Vidal et al. [44]	Beam B	7.3	10.3	18.52	20	17.36	-13.2
Alonso et al. [45]	Series-1	7.6	6.85	16.6	15.14	12.97	-14.4
	Series-1	9.7	9.62	19.82	24.86	24.89	0.1
Torres-Acosta [46]	CPG1	12.8	11.93	22.51	32	35.28	10.3
Andrade et al. [47]	A1	10	9.2	19.33	16	17.47	9.17
Torres-Acosta and Sagues [48]	C3	9.3	16.42	25.53	61.3	65.44	6.76
	C4	9.3	16.42	25.46	54.4	63.21	16.2
	C7	9.3	16.42	25.54	72.8	65.0	-10.7

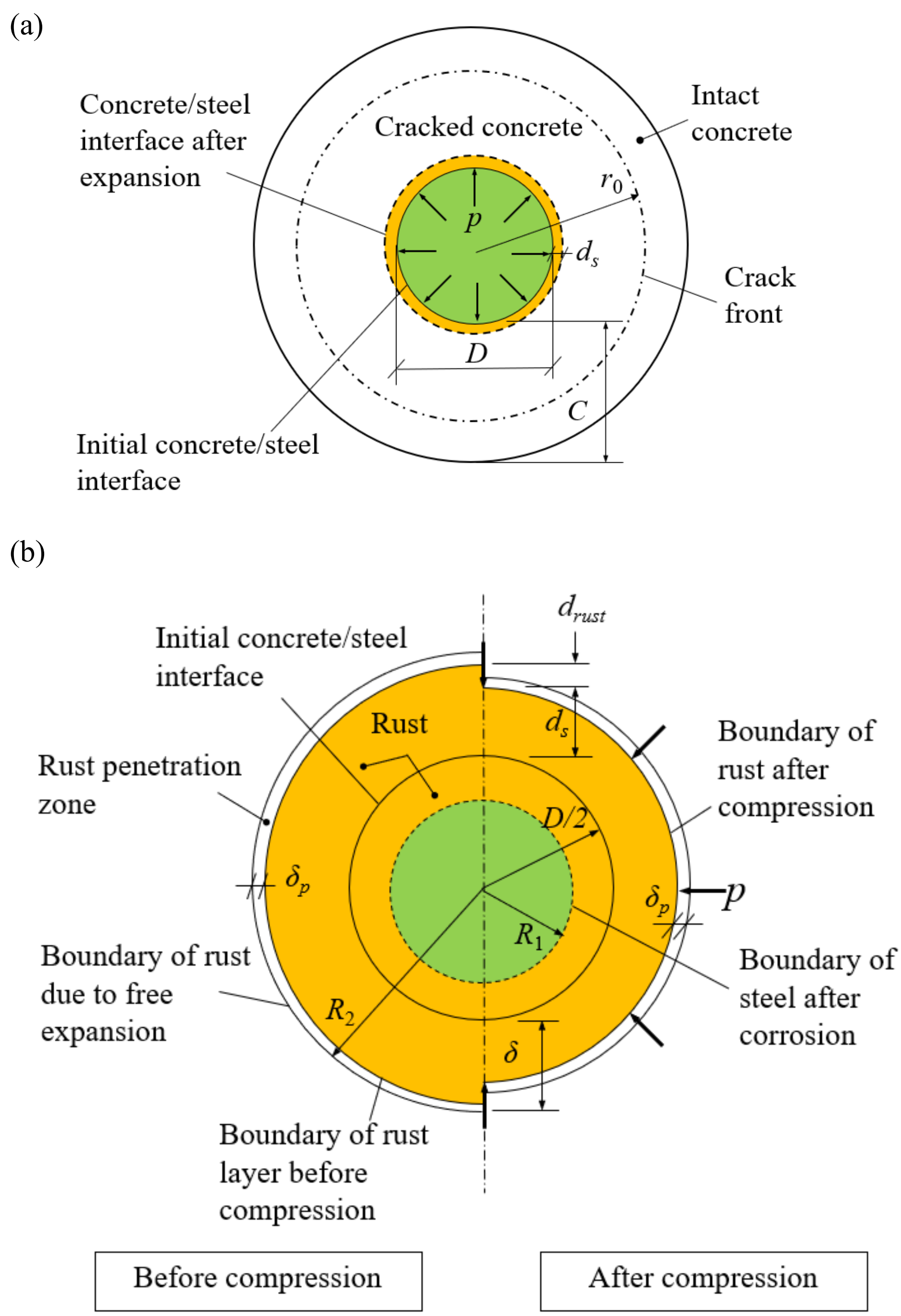

Fig. 1. Schematic of displacement-based inverse analysis method: (a) concrete cracking due to rebar corrosion and (b) expansion of rust before and after compression.

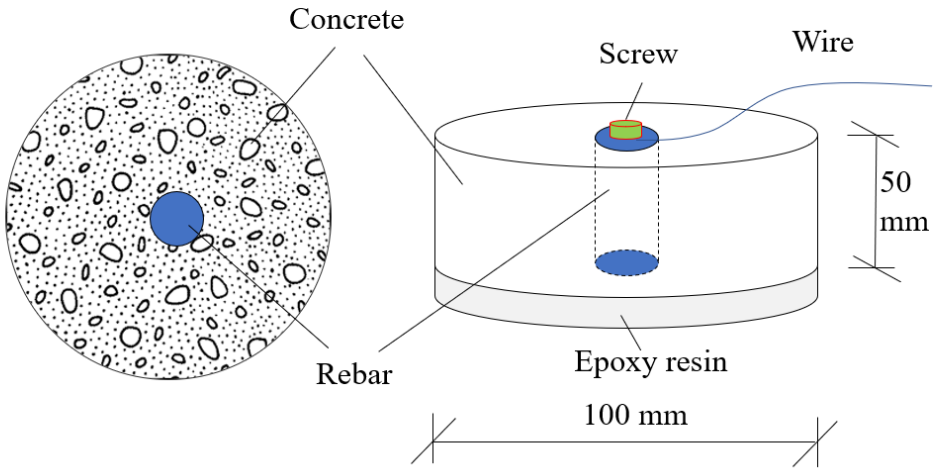

Cylindrical specimens with dimensions of 100 mm × 50 mm.

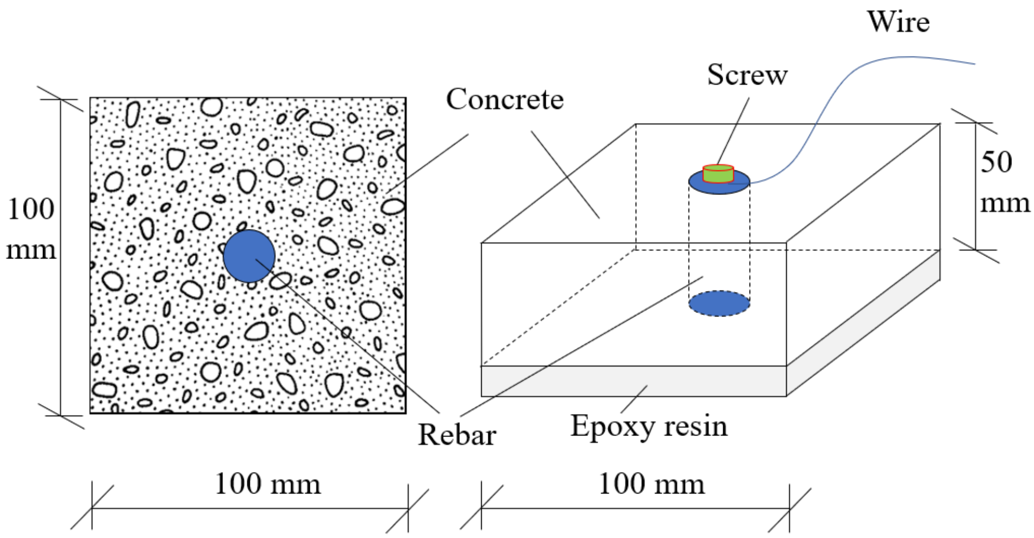

Square specimens of 100 mm × 100 mm × 50 mm.

Fig. 2. Dimensions and details of preparing specimen.

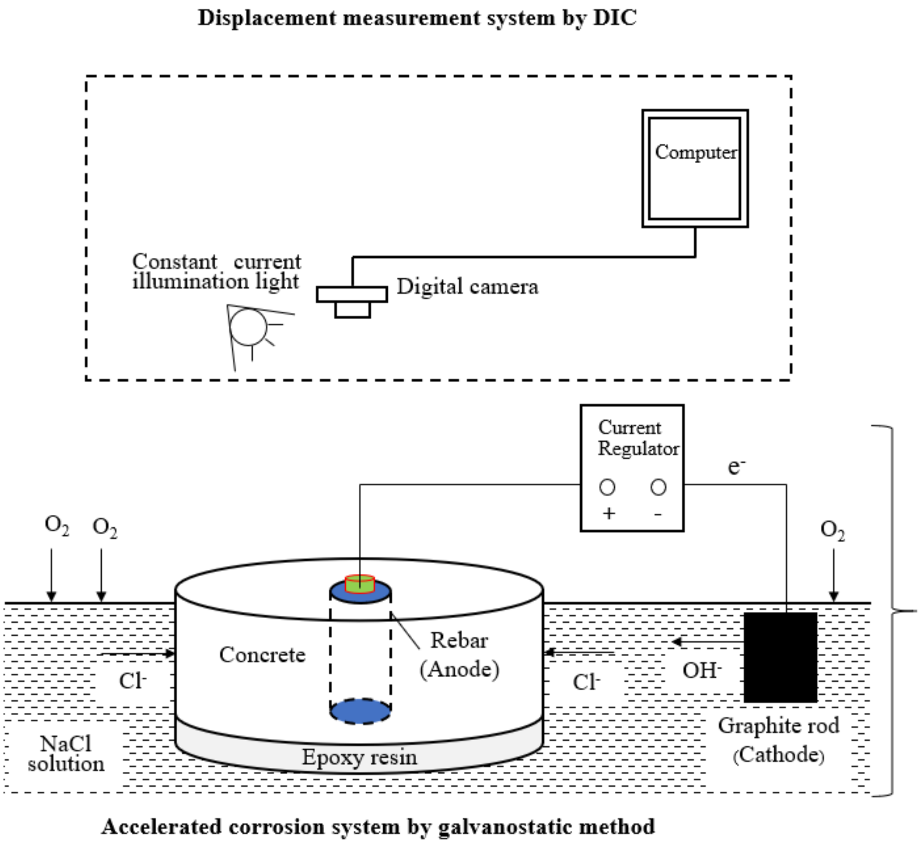

Fig. 3. Illustration of experimental setup with accelerated corrosion system by using galvanostatic method and displacement measurement system of DIC.

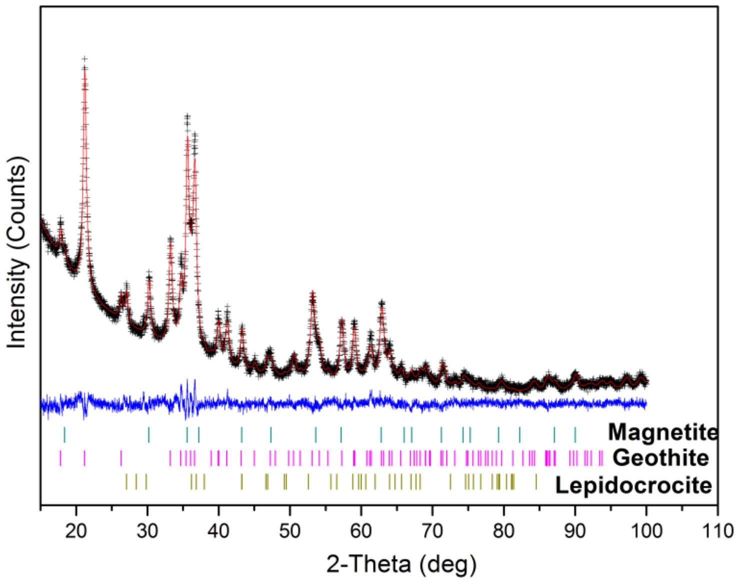

Fig. 4. Measured XRD spectra of rust.

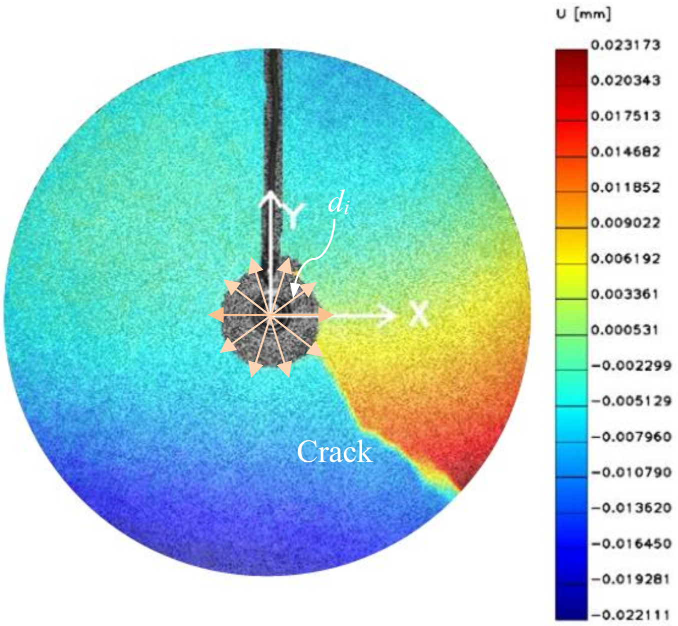

(a) Measured displacement in X-direction.

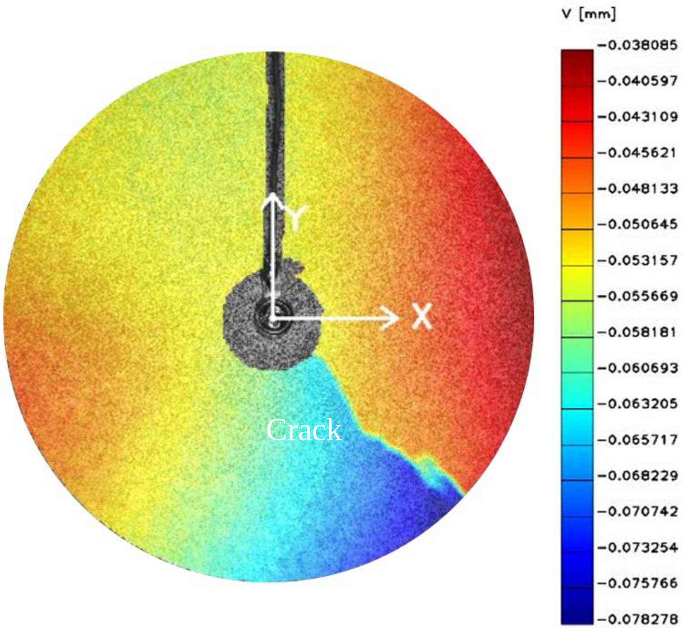

(b) Measured displacement in Y-direction.

Fig. 5. Measured displacement of U5 with DIC.

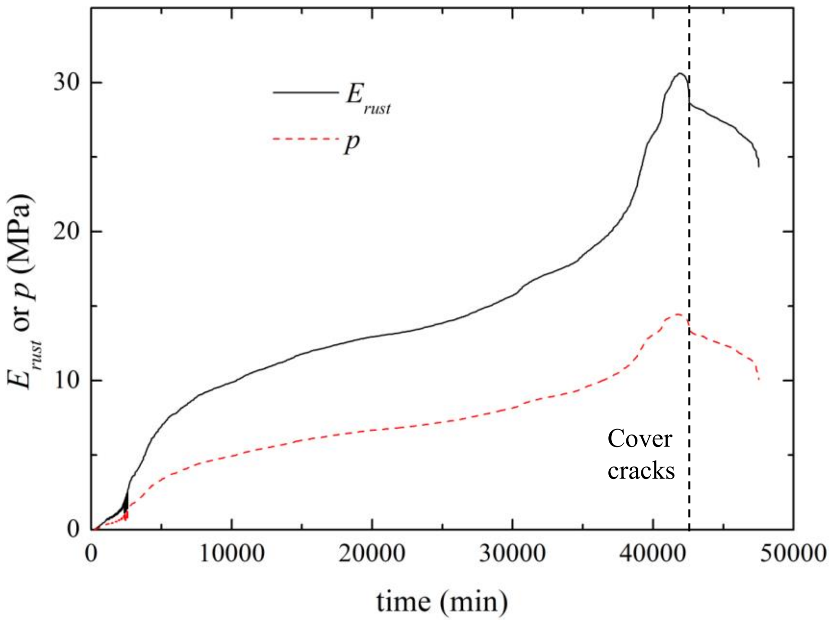

Fig. 6. Change in p and E_{rust} of U1 specimen versus time.

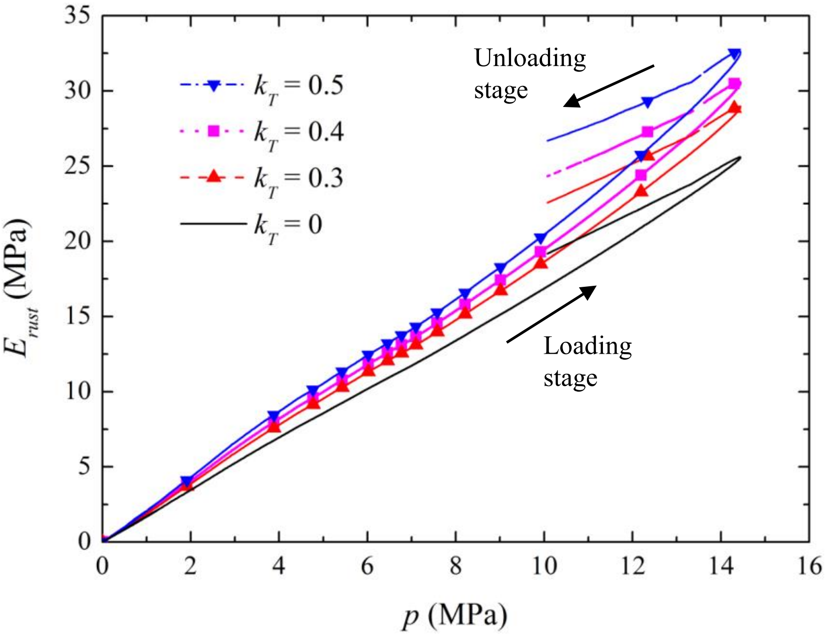

Fig. 7. Change in evaluated E_{rust} with p in U1 specimen for different parameters of k_T.

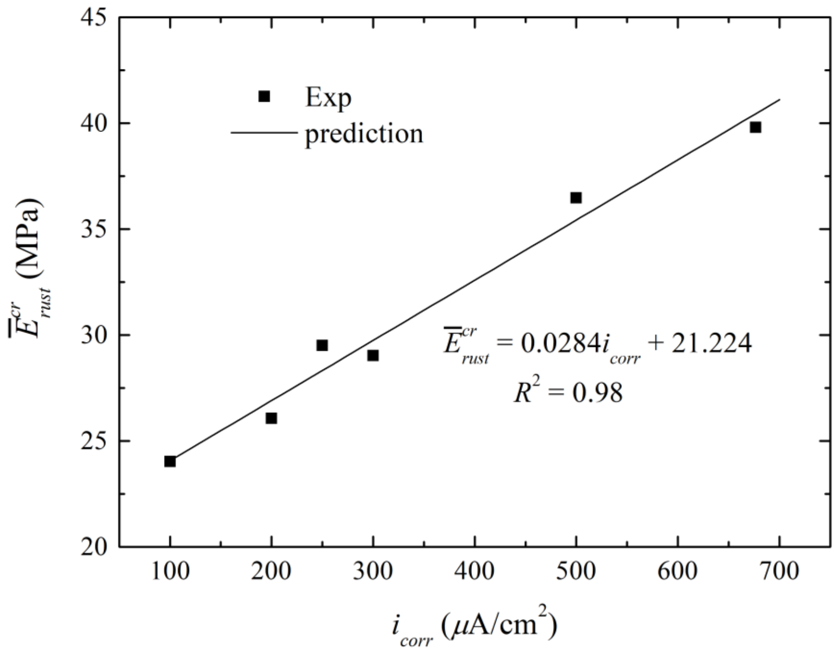

(a)

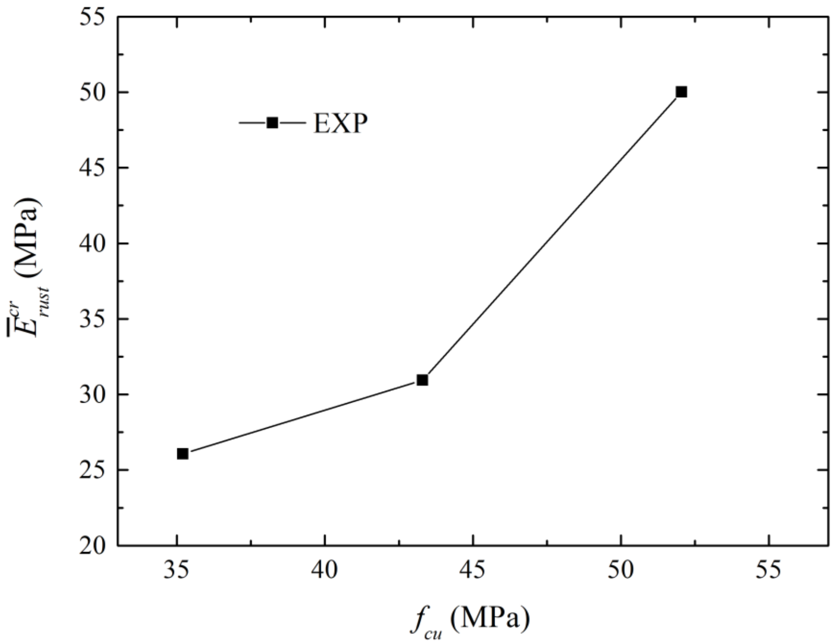

(b)

Fig. 8. Variation of $\overline{E}_{rust}^{cr}$ versus (a) i_{corr} and (b) f_{cu}.

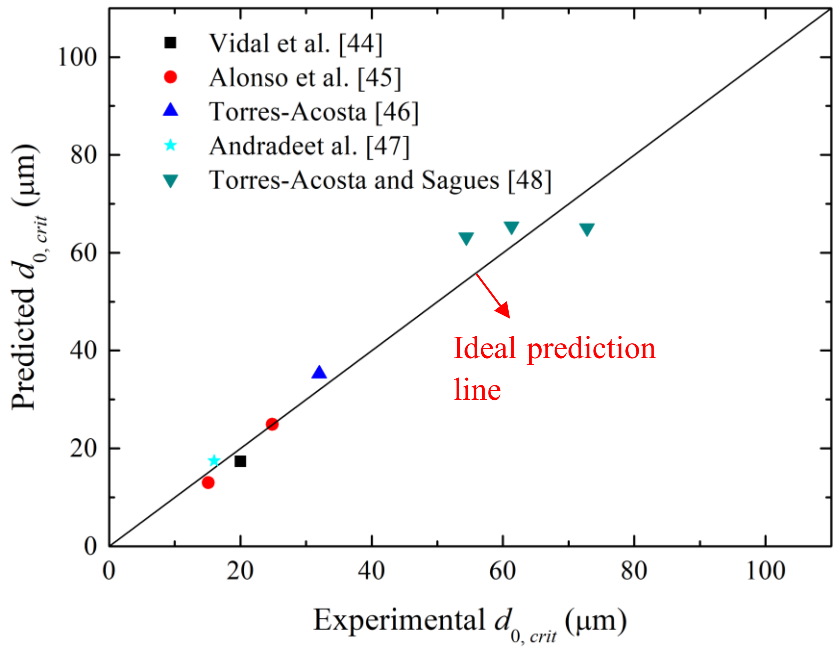

Fig. 9. Validation of predicted $d_{0,\text{ crit}}$ with Eq. (16).